

# Unveiling a New $\beta$ -Scaling of the Tearing Instability in Weakly Collisional Plasmas

Gabriel L. Ferreira-Santos\*

*Astrophysics Division at National Institute for Space Research - INPE, São José dos Campos, SP, Brazil*

Grzegorz Kowal<sup>†</sup> and Diego A. Falceta-Gonçalves<sup>‡</sup>

*Escola de Artes, Ciências e Humanidades, University of São Paulo - EACH-USP, São Paulo, SP, Brazil*

(Dated: March 18, 2025)

We investigate the linear tearing instability in weakly collisional, gyrotropic plasmas via a non-ideal CGL-MHD framework. Even for an initially isotropic equilibrium, our analysis reveals a striking dependence of the maximum growth rate on plasma- $\beta$ , with  $\gamma_{\max}\tau_A \propto \beta^{-1/4}$  in the high- $\beta$  regime—thereby challenging the  $\beta$ -independence predicted by standard MHD theory. We show that this new scaling emerges from the self-consistent fluctuations in pressure anisotropy, which can suppress or enhance the instability depending on the underlying plasma parameters. Systematic scans of the Lundquist number, magnetic Prandtl number, and anisotropy degree  $\Delta\beta$  highlight conditions under which the tearing mode departs significantly from classical behavior. Our findings emphasize that weak collisionality and gyrotropic effects must be considered to accurately capture tearing evolution in high- $\beta$  plasma environments.

*Introduction* – The tearing mode instability, a resistive MHD process first analyzed by Furth, Killeen, and Rosenbluth in 1963 (FKR63) [1], leads to the destabilization of a planar current sheet at the vanishing loci of antiparallel components of a magnetic field, and the formation of plasmoids. Their analysis demonstrated that the growth rate scales as  $\gamma \propto S^{-3/5}$  in the short-wavelength regime and as  $\gamma \propto S^{-1/3}$  in the long-wavelength regime, where  $S = aV_A/\eta$  is the Lundquist number, with  $V_A$  being the characteristic Alfvén speed,  $a$  the thickness of the current sheet, and  $\eta$  the magnetic resistivity. Furthermore, FKR63 demonstrated that the maximum growth rate satisfies  $\gamma_{\max}\tau_a \sim S^{-1/2}$  and  $k_{\max}a \sim S^{-1/4}$ , where  $\tau_a = a/V_A$  is the Alfvén time. Within the incompressible magnetohydrodynamic (MHD) framework, the maximum growth rate and wavenumber of the tearing instability are *independent of the plasma- $\beta$* , which is defined as the ratio of thermal pressure to magnetic pressure.

Since the pioneering work of FKR63, the linear tearing mode instability has been extensively studied in planar geometry, incorporating various physical effects relevant to laboratory and astrophysical plasmas. In the MHD regime, the inclusion of 3D geometry and a guide field introduces multiple resonant surfaces within the current sheet, enabling oblique mode growth absent in 2D configurations, while a strong guide field can suppress normal variations in the eigenfunctions and modify wave propagation, particularly in the presence of Hall effects [2–4]. Viscosity stabilizes the instability in certain regimes [5], and for large magnetic Prandtl numbers,  $Pr_m = \nu/\eta$ , the fastest-growing mode follows the scaling laws  $\gamma_{\max}\tau_a \sim Pr_m^{-1/4}$  and  $k_{\max}a \sim Pr_m^{1/8}$  [6]. Additionally, local velocity shear influences stability conditions [5, 7, 8]. However, these studies remain within the MHD approximation, assuming pressure isotropy due to high collisionality.

Observational data from space plasmas confirm their

predominantly collisionless nature. Missions such as ESA’s Cluster [9] and NASA’s THEMIS and MMS [10, 11] have resolved kinetic-scale processes, including magnetic reconnection and turbulence, while the Van Allen Probes [12] revealed collisionless wave-particle interactions in the radiation belts. Observations from the Parker Solar Probe further substantiate this paradigm, demonstrating the prevalence of gyrotropy in the solar wind [13–15].

Traditional MHD studies of tearing instabilities in astrophysical plasmas often neglect pressure anisotropy in collisionless regimes [16–18], despite the fact that a gyrotropic pressure tensor alters wave dynamics compared to isotropic models [19]. Sonnerup [20] demonstrated that under high plasma- $\beta$  conditions, tearing instability is suppressed in symmetric current sheets. Chiou and Hau [21–23] expanded this framework, showing that anisotropic plasmas exhibit two critical behaviors: (i) a transition from exponential to oscillatory tearing modes when the perpendicular-to-parallel pressure ratio exceeds a critical threshold, accompanied by enhanced growth rates, and (ii) a paradoxical increase in growth rate with the magnetic Reynolds number under specific conditions—directly contradicting classical tearing theory.

While standard MHD-based tearing instability theories are widely applied to space plasmas, they fail to account for prevalent pressure anisotropy. This work addresses the critical question: *How does tearing instability evolve in gyrotropic plasmas?* By extending the analysis to a non-ideal CGL-MHD framework [24], we systematically quantify the effects of anisotropy on growth rates. Our primary objective is to determine whether classical parameter dependencies—on plasma- $\beta$ , the Lundquist number  $S$ , the anisotropy degree  $\Delta\beta = \beta_{\parallel} - \beta_{\perp}$ , and the magnetic Prandtl number  $Pr_m$ —remain unchanged or vary in this gyrotropic regime.

This paper is organized as follows. First, we discuss

the linearization of the non-ideal gyrotropic CGL-MHD equations. Next, we outline the simulation setup and pseudo-spectral methods used to solve the eigenvalue problem. We then present our results and conclude with a discussion of implications and future research directions.

*Governing Equations and Linearization* – We present the governing equations of the non-ideal gyrotropic CGL-MHD model, which serve as the basis for analyzing tearing instability in magnetized plasmas with gyrotropic pressure. Assuming the incompressible limit ( $\nabla \cdot \mathbf{v} = 0$ ), these equations take the following form:

$$\frac{\partial \mathbf{v}}{\partial t} + (\mathbf{v} \cdot \nabla) \mathbf{v} = -\nabla \cdot (p_{\perp} \mathbf{I} + \Delta p \mathbf{b}\mathbf{b}) + \mathbf{J} \times \mathbf{B} + \nu \nabla^2 \mathbf{v} \quad (1)$$

$$\frac{\partial \mathbf{B}}{\partial t} = \nabla \times (\mathbf{v} \times \mathbf{B}) + \eta \nabla^2 \mathbf{B}, \quad \nabla \cdot \mathbf{B} = 0 \quad (2)$$

where  $\mathbf{v}$  and  $\mathbf{B}$  represent the velocity and magnetic field, respectively;  $\mathbf{J} = \nabla \times \mathbf{B}$  is the current density;  $\Delta p = p_{\parallel} - p_{\perp}$ , where  $p_{\parallel}$  and  $p_{\perp}$  are the pressure components parallel and perpendicular to the magnetic field, respectively;  $\mathbf{b} \equiv \mathbf{B}/|\mathbf{B}|$ ; and  $\nu$  and  $\eta$  denote viscosity and magnetic resistivity, respectively.

The non-ideal CGL-MHD equations for gyrotropic plasmas are closed by incorporating the evolution equations for the two pressure tensor components, as described in [25]:

$$\begin{aligned} \frac{\partial p_{\parallel}}{\partial t} + (\mathbf{v} \cdot \nabla) p_{\parallel} = & -(\gamma_{\parallel} - 1) p_{\parallel} [\mathbf{b} \cdot (\mathbf{b} \cdot \nabla \mathbf{v})] \\ & + \eta (\gamma_{\parallel} - 1) (\mathbf{b} \cdot \mathbf{J})^2 + \frac{1}{3} \nu (\gamma_{\parallel} - 1) (\nabla \times \mathbf{v})^2 \end{aligned} \quad (3)$$

$$\begin{aligned} \frac{\partial p_{\perp}}{\partial t} + (\mathbf{v} \cdot \nabla) p_{\perp} = & (\gamma_{\perp} - 1) p_{\perp} [\mathbf{b} \cdot (\mathbf{b} \cdot \nabla \mathbf{v})] \\ & + \eta (\gamma_{\perp} - 1) [\mathbf{J} \cdot \mathbf{J} - (\mathbf{b} \cdot \mathbf{J})^2] + \frac{2}{3} \nu (\gamma_{\perp} - 1) (\nabla \times \mathbf{v})^2 \end{aligned} \quad (4)$$

where  $\gamma_{\parallel}$  and  $\gamma_{\perp}$  are the adiabatic indices along and across the magnetic field, respectively. In this work, we assume a 2.5D geometry (XZ-plane), where all  $y$ -derivatives are zero. Moreover, we consider the double-adiabatic case ( $\gamma_{\parallel} = 3$ ,  $\gamma_{\perp} = 2$ ).

The current sheet is defined by an equilibrium magnetic field  $\mathbf{B}_0 = B_0(z) \hat{\mathbf{i}} + B_g(z) \hat{\mathbf{j}}$ , where  $B_0(z) = \tanh(z/a)$  and  $B_g(z) = \text{sech}(z/a)$ , ensuring that  $|\mathbf{B}_0|^2 = 1$ . The parameter  $a$  represents the current sheet thickness and is set to unity in our analysis. The equilibrium profiles for parallel and perpendicular pressure are uniform. Specifically, the parallel pressure is given by  $p_{\parallel,0} = \frac{1}{2} \beta_0 + \frac{1}{2} \Delta \beta_0$ , while the perpendicular pressure is  $p_{\perp,0} = \frac{1}{2} \beta_0$ , where  $\beta_0$  and  $\Delta \beta_0$  are prescribed parameters. We should note that, in order to ensure  $p_{\parallel} > 0$ , we impose the condition  $\Delta \beta_0 > -\beta_0$ . The equilibrium velocity is zero everywhere.

Linearizing the CGL-MHD equations around this equilibrium we assume small perturbations of the form

$\delta f(t, \mathbf{r}) = \delta f(z) \exp[ikx + \gamma t]$ , where  $k$  and  $\gamma$  denote the wave vector's x-component and the growth rate of a given mode, respectively. The linearization of Eqs. 1-4 yields five coupled equations governing the perturbations of velocity, magnetic field, and pressure difference  $\Delta p$  (see Appendix A).

To analyze the stability of the linearized CGL-MHD equations, we employ the *Pseudo-Spectral Eigenvalue Calculator with an Automated Solver* (PSECAS) framework [26], which efficiently solves eigenvalue problems arising in fluid and plasma stability analyses. First, we express the linearized CGL-MHD equations in a matrix form, where perturbations are expanded as normal modes in the form described above, reducing the problem to a set of coupled ordinary differential equations (ODEs) in  $z$ . PSECAS discretizes these ODEs using a pseudo-spectral collocation method on a non-uniform grid optimized for resolving steep gradients, mapping the problem onto a generalized eigenvalue problem. It then systematically increases the resolution of the eigenproblem matrices and verifies the convergence of the computed growth rates to ensure numerical accuracy. The resulting eigenvalue spectrum provides the growth rates ( $\gamma$ ) and mode structures of tearing instability under different equilibrium conditions, allowing us to systematically investigate the effects of plasma- $\beta$ , pressure anisotropy, viscosity and resistivity on stability in the CGL-MHD framework.

*Results* – To evaluate the influence of key equilibrium parameters on the maximum growth rate and wavenumber of the tearing instability, we conducted a systematic study. We considered the plasma- $\beta$ , the anisotropy degree  $\Delta \beta$ , the magnetic Prandtl number  $Pr_m$ , and the Lundquist number  $S$ .

First, by fixing the magnetic Prandtl number at unity ( $Pr_m = 1$ ) and setting the anisotropy degree to zero ( $\Delta \beta = 0$ ), we varied the plasma- $\beta$  values from  $10^{-2}$  to  $10^2$  for different Lundquist numbers:  $10^4$ ,  $10^5$ , and  $10^6$ . The upper panel of Figure 1 presents the maximum growth rate and the corresponding wavelength of the tearing instability as functions of the equilibrium plasma- $\beta$ . Solid lines represent the gyrotropic CGL-MHD model, while dashed lines correspond to classical MHD. In particular, we identify a new plasma- $\beta$  dependence for the CGL-MHD case, characterized by a scaling of  $\sim \beta^{-1/4}$  in the high- $\beta$  regime ( $\beta \gg 1$ ). This new dependence arises (even for  $\Delta \beta_0 = 0$ ) as velocity and B-field fluctuations give rise to pressure anisotropy ( $\Delta p$ ) fluctuations, as may be noticed from the first term in the RHS of Eq. 9. This effect is not seen in standard MHD, given that  $\Delta p = 0$  is a fixed condition. Furthermore, as shown in the upper right plot of Figure 1, the maximum growth rate shifts to larger spatial scales as  $\beta$  increases.

In addition to the  $\beta$ -dependence, we also analyzed the dependence on the magnetic Prandtl number, as shown in the lower panel of Figure 1. For this analysis the Lundquist number is fixed at  $10^4$  and varied  $Pr_m$  over

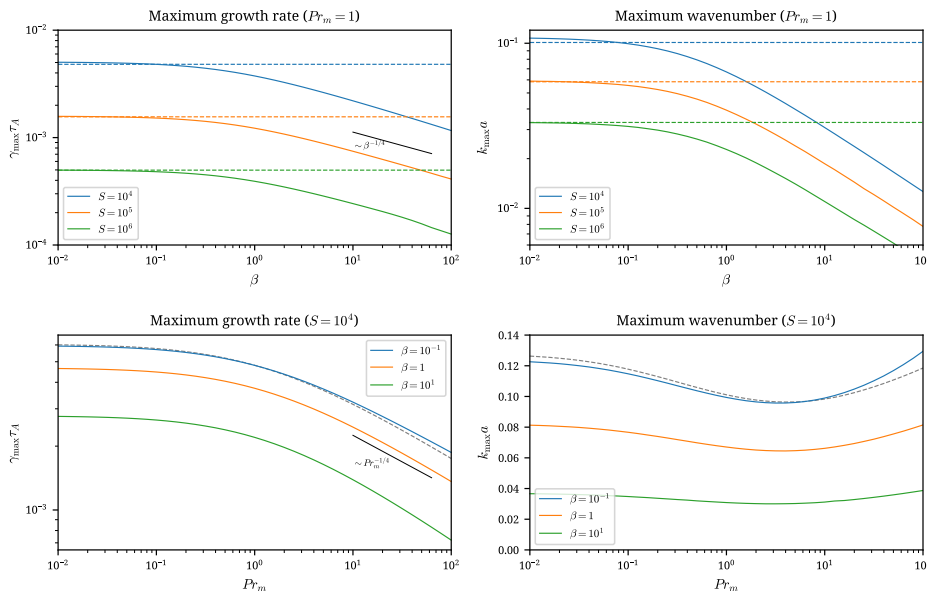


FIG. 1. Maximum growth rate and the corresponding maximum wavenumber of the tearing mode instability as functions of the equilibrium plasma- $\beta$  parameter (top) and the magnetic Prandtl number,  $Pr_m$ , (bottom). The analysis considers both the MHD framework (dashed lines) and the gyrotropic CGL-MHD model. Moreover, the influence of the Lundquist number,  $S$ , is examined. For plasma- $\beta$  dependence, we set  $Pr_m = 1$  and  $\Delta\beta = 0$ . The Prandtl number dependence was analyzed for  $S = 10^4$  and  $\Delta\beta = 0$ . In collisionless plasmas, the tearing mode growth rate scales close to  $\beta^{-1/4}$  for  $\beta \gg 1$ . For  $Pr_m \gg 1$ , the Prandtl number dependence is similar to the MHD case.

the range  $10^{-2}$  to  $10^2$  for three plasma- $\beta$  values:  $10^{-1}$ , 1, and 10. The plots reveal that the magnetic Prandtl number dependence,  $\sim Pr_m^{-1/4}$ , is consistent with the scaling reported by [6]. In both the MHD and CGL-MHD frameworks, an increase in  $Pr_m$  leads to a reduction in the maximum growth rate due to enhanced viscous dissipation, which suppresses energy transfer. For higher plasma- $\beta$ , the  $\sim Pr_m^{-1/4}$  scaling appears to be preserved for  $Pr_m \gg 1$ , though the additional  $\beta$  effect, discussed earlier, weakens the magnetic tension and shifts the instability curves downward.

Next, with the magnetic Prandtl number fixed at unity ( $Pr_m = 1$ ), we examined the effects of varying the equilibrium pressure anisotropy  $\Delta\beta$  for two plasma- $\beta$  values ( $\beta = 1$  and 10) and three Lundquist numbers ( $S = 10^4$ ,  $10^5$ , and  $10^6$ ). To ensure positive parallel pressure,  $\Delta\beta$  was varied between  $-1$  and  $1.5$  for  $\beta = 1$ , and between  $-1.5$  and  $1.5$  for  $\beta = 10$ . The results are presented in Figure 2, where the maximum growth rate and corresponding wavenumber for the classical MHD case are marked with points.

In the CGL-MHD framework, when  $\Delta\beta > 0$ , the tearing instability growth rate is further suppressed compared to the MHD model. Conversely, for  $\Delta\beta < 0$ , the effect of plasma- $\beta$  can be counteracted, potentially leading to higher growth rates than in MHD. However, this behavior strongly depends on the plasma- $\beta$  value. For  $\beta = 1$ , enhanced growth relative to MHD occurs

only when the perpendicular pressure dominates (i.e.,  $\Delta\beta < 0$ ), whereas for  $\Delta\beta > 0$ , the CGL-MHD model consistently predicts lower growth rates. Thus, under specific conditions—low plasma- $\beta$  combined with  $\Delta\beta < 0$ —a collisionless plasma may experience tearing instability growth rates exceeding those predicted by conventional MHD.

The results above demonstrate that in the gyrotropic CGL-MHD model, the tearing instability growth rate decreases as  $\beta$  increases ( $\beta \gg 1$ ), leading to lower growth rates compared to standard MHD. This effect, relevant in high- $\beta$  environments such as the solar corona, arises from stabilizing forces in the momentum equation, and reduced magnetic tension. Additionally, the wavelength of the fastest-growing mode increases, as thermal pressure confines perturbations and weakens magnetic tension, restricting tearing modes to larger spatial scales. In the low- $\beta$  regime, the CGL-MHD model recovers the MHD limit, showing very weak dependence on  $\beta$ . However, for high plasma- $\beta$ , we observe an asymptotic scaling  $\gamma_{max}\tau_A \sim \beta^{-1/4}$ , even for isotropic equilibrium conditions ( $\Delta\beta = 0$ ).

Unlike standard MHD, where pressure anisotropy does not affect tearing modes, the collisionless CGL-MHD framework permits fluctuations in  $\Delta p = p_{\parallel} - p_{\perp}$  due to the exchange between  $p_{\parallel}$  and  $p_{\perp}$  as  $\mathbf{B}$  and  $\mathbf{v}$  fluctuate. Since Eq. 9 shows that  $\Delta\delta p$  explicitly depends on  $\beta$ , this reveals a physical mechanism that introduces a growth rate dependence on  $\beta$ , even in an initially isotropic equi-

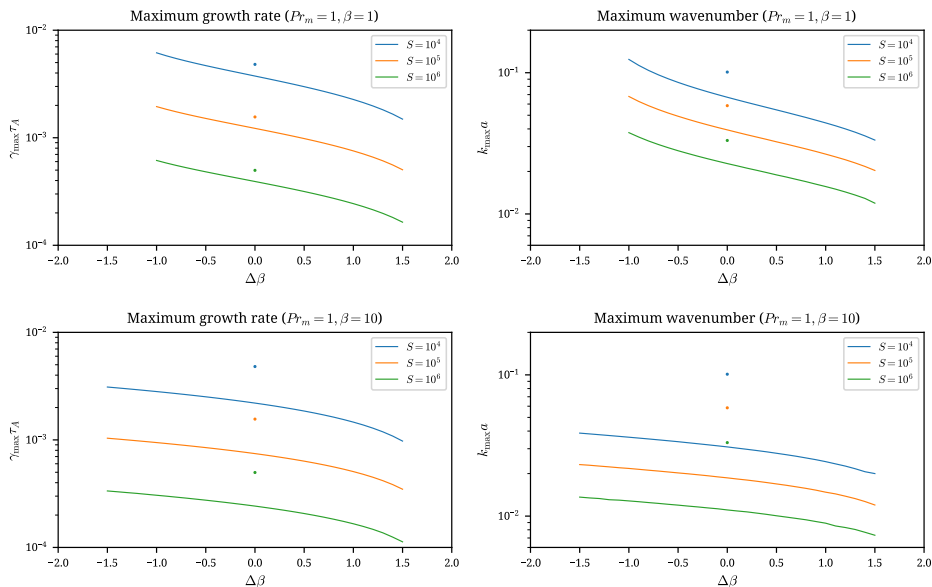


FIG. 2. Maximum growth rate and maximum wavenumber of the tearing instability versus the equilibrium pressure anisotropy parameter,  $\Delta\beta$  as a function of  $\Delta\beta$  for  $\beta = 1$  and  $10$  (upper and bottom row, respectively). Each panel displays three curves corresponding to Lundquist numbers  $S = 10^4$ ,  $10^5$ , and  $10^6$ , with  $Pr_m = 1$ . The points represent the growth rate values obtained from the MHD model for each  $S$  tested with  $\Delta\beta = 0$ .

librium.

*Conclusions* – This study investigates the stability of the tearing mode in a collisionless plasma using the gyrotronic CGL-MHD framework, extending classical MHD analyses to include pressure anisotropy effects. By linearizing the non-ideal CGL-MHD equations and solving the resulting eigenvalue problem with a pseudo-spectral method, we systematically examine the dependence of the tearing mode growth rate on plasma- $\beta$ , pressure anisotropy  $\Delta\beta$ , the magnetic Prandtl number  $Pr_m$ , and the Lundquist number  $S$ . Our study leads to several key conclusions, which can be summarized as follows:

- Relaxing the pressure isotropy assumption from the MHD approximation significantly modifies the tearing instability, introducing a dependence of its growth rate on plasma- $\beta$ . In the gyrotronic CGL-MHD framework, the maximum growth rate in high- $\beta$  plasmas follows a  $\beta^{-1/4}$  scaling for  $\beta \gg 1$ . Even for an initially isotropic equilibrium ( $p_{\parallel} = p_{\perp}$ ), standard MHD predictions are not recovered, suggesting additional suppression mechanisms in collisionless and weakly collisional plasmas. Furthermore, higher plasma- $\beta$  values decrease the maximum wavenumber of unstable modes, restricting tearing instability to larger spatial scales.
- In the CGL-MHD framework, the maximum growth rate and corresponding wavenumber are highly sensitive to the degree of equilibrium anisotropy. When  $p_{\parallel} > p_{\perp}$ , the tearing instability is suppressed, whereas for  $p_{\parallel} < p_{\perp}$ , plasma-

$\beta$  effects can be counteracted, potentially enhancing growth in low- $\beta$  ( $\beta \lesssim 1$ ) conditions, leading to faster instability development compared to MHD. In higher- $\beta$  plasmas, the dependence of the growth rate on  $\Delta p$  becomes weaker, while the most unstable modes shift to larger spatial scales.

- The effects of viscosity are similar to those in the MHD approximation, providing an additional contribution to suppressing the instability, with the growth rate following the expected scaling of  $\sim Pr_m^{-1/4}$ .

These findings challenge the assumption that tearing instability dominates in high- $\beta$ , weakly collisional plasmas such as the solar corona. In CGL-MHD, tearing evolves much slower than in standard MHD—except for low- $\beta$  cases with  $\beta_{\parallel} < \beta_{\perp}$ —suggesting that other mechanisms drive reconnection in astrophysical settings. This framework is also relevant to the intracluster medium and early magnetic field amplification [27]. Future work will extend this analysis to 3D CGL-MHD, where oblique modes, flux ropes, and compressibility further shape tearing dynamics.

The authors acknowledge support from FAPESP (grants 2013/10559-5, 2021/02120-0, 2021/06502-4, and 2022/03972-2) and CAPES. The simulations presented in this work were performed using the clusters of the Group of Theoretical Astrophysics at EACH-USP (Hydra HPC), which was acquired with support from FAPESP (grants 2013/04073-2 and 2022/03972-2).

## Appendix A: Linearization of the CGL-MHD Equations

In this appendix, we present the detailed linearization of the CGL-MHD equations, which govern the evolution of an anisotropic plasma in the presence of a guiding magnetic field. The derivation follows the standard approach of expanding the equations around an equilibrium configuration and retaining only first-order perturbations. Compared to the standard MHD framework, the key difference in CGL-MHD lies in the inclusion of the gyrotropic pressure tensor, introducing additional terms that influence the system's stability. We begin by linearizing the momentum equation, highlighting the effects of pressure anisotropy. Subsequently, we derive the linearized pressure difference equation, accounting for contributions from equilibrium anisotropy, Ohmic heating, and viscosity. Finally, we obtain the full set of coupled linearized equations governing the evolution of velocity, magnetic field, and pressure perturbations, which serve as the basis for the stability analysis presented in the main text.

When considering the momentum equation, the difference between the MHD and CGL-MHD approximations stems from the introduction of the pressure tensor in the latter. This causes the pressure term to become

$$\nabla \cdot [p_{\perp} \mathbf{I} + (p_{\parallel} - p_{\perp}) \mathbf{b}\mathbf{b}],$$

where  $p_{\parallel}$  and  $p_{\perp}$  are the parallel and perpendicular components of the pressure tensor, and  $\mathbf{b} \equiv \mathbf{B}/|\mathbf{B}|$ . Applying vector identities, the anisotropic component of the above term can be expressed as

$$(\mathbf{B} \cdot \nabla) \left( \frac{\Delta p}{|\mathbf{B}|^2} \mathbf{B} \right),$$

where  $\Delta p \equiv p_{\parallel} - p_{\perp}$ .

Since our equilibrium field has unit magnitude everywhere,  $|\mathbf{B}_0| = 1$ , and applying the Taylor expansion of the inverse magnetic field magnitude for small magnetic field perturbation,  $|\delta\mathbf{B}| \ll 1$ ,

$$\frac{1}{|\mathbf{B}|^2} = \frac{1}{(\mathbf{B}_0 + \delta\mathbf{B}) \cdot (\mathbf{B}_0 + \delta\mathbf{B})} \approx 1 - 2(\mathbf{B}_0 \cdot \delta\mathbf{B}),$$

the resulting linearized pressure anisotropy term is:

$$\begin{aligned} (\mathbf{B} \cdot \nabla) \left( \frac{\Delta p}{|\mathbf{B}|^2} \mathbf{B} \right) &\approx (\mathbf{B}_0 \cdot \nabla) (\mathbf{B}_0 \delta\Delta p) \\ &+ \Delta p_0 \{ (\mathbf{B}_0 \cdot \nabla) \delta\mathbf{B} + (\delta\mathbf{B} \cdot \nabla) \mathbf{B}_0 \\ &- 2(\mathbf{B}_0 \cdot \nabla) [\mathbf{B}_0 (\mathbf{B}_0 \cdot \delta\mathbf{B})] \} \end{aligned}$$

To eliminate the pressure contribution in the linearized MHD equations, the momentum equation is transformed into the vorticity equation by applying the curl operator

to all terms. In the CGL-MHD equations, the curl removes the contribution from the perpendicular pressure; however, the anisotropic pressure component does not vanish. Therefore, the curl operator must be applied to the linearized anisotropic pressure term, as shown above.

We observe two principal contributions to this resulting term: the first term on the right-hand side, which describes the effects of pressure anisotropy perturbation, and the remaining terms, which are non-negligible when the equilibrium exhibits pressure anisotropy. Consequently, it is necessary to consider the pressure equations. However, because only pressure differences are relevant, we linearize the equation for the pressure difference, as shown below, rather than linearizing equations for parallel and perpendicular pressure separately:

$$\begin{aligned} \frac{\partial \Delta p}{\partial t} &= -(\mathbf{v} \cdot \nabla) \Delta p - (3p_{\perp} + 2\Delta p) [\mathbf{b} \cdot (\mathbf{b} \cdot \nabla) \mathbf{v}] \\ &+ \eta \left[ 3(\mathbf{b} \cdot \mathbf{J})^2 - (\mathbf{J} \cdot \mathbf{J}) \right] + \frac{2}{3} \nu |\nabla \times \mathbf{v}|^2 \end{aligned}$$

Linearizing the equation above, we immediately notice that the advection and viscous terms vanish, since our equilibrium field has  $\mathbf{v}_0 = \mathbf{0}$ . The second term on the right-hand side requires additional attention. The scalar products involving the magnetic field direction,  $\mathbf{b}$ , can be rewritten as

$$\mathbf{b} \cdot (\mathbf{b} \cdot \nabla) \mathbf{v} = \frac{1}{|\mathbf{B}|^2} [\mathbf{B} \cdot (\mathbf{B} \cdot \nabla) \mathbf{v}].$$

Applying the Taylor expansion of the inverse squared magnetic field magnitude, as shown previously, the resulting linearization of this term simplifies, largely due to the null equilibrium velocity field, to a simple form:

$$\mathbf{b} \cdot (\mathbf{b} \cdot \nabla) \mathbf{v} \approx \mathbf{B}_0 \cdot (\mathbf{B}_0 \cdot \nabla) \delta\mathbf{v}.$$

The final part is the linearization if this equations is the Ohmic heating. We have two terms there, namely,  $(\mathbf{b} \cdot \mathbf{J})^2$  and  $(\mathbf{J} \cdot \mathbf{J})$ . Focusing on the first term, we can rewrite it as  $(\mathbf{B} \cdot \mathbf{J})^2 / |\mathbf{B}|^2$ , and using the approximation of  $1/|\mathbf{B}|^2$  obtained the linearized version of it

$$\begin{aligned} (\mathbf{b} \cdot \mathbf{J})^2 &\approx 2(\mathbf{B}_0 \cdot \mathbf{J}_0) [(\mathbf{B}_0 \cdot \delta\mathbf{J}) + (\mathbf{J}_0 \cdot \delta\mathbf{B}) \\ &- (\mathbf{B}_0 \cdot \mathbf{J}_0) (\mathbf{B}_0 \cdot \delta\mathbf{B})] \end{aligned}$$

The second term reduces to

$$(\mathbf{J} \cdot \mathbf{J}) \approx 2(\mathbf{J}_0 \cdot \delta\mathbf{J}).$$

Putting all together the linearized pressure difference equation results in

$$\begin{aligned} \frac{\partial \delta\Delta p}{\partial t} &= - \left( \frac{3}{2} \beta_0 + \Delta\beta_0 \right) [\mathbf{B}_0 \cdot (\mathbf{B}_0 \cdot \nabla) \delta\mathbf{v}] \\ &+ \eta \{ 6(\mathbf{B}_0 \cdot \mathbf{J}_0) [(\mathbf{B}_0 \cdot \delta\mathbf{J}) + (\mathbf{J}_0 \cdot \delta\mathbf{B}) \\ &- (\mathbf{B}_0 \cdot \mathbf{J}_0) (\mathbf{B}_0 \cdot \delta\mathbf{B})] - 2(\mathbf{J}_0 \cdot \delta\mathbf{J}) \} \end{aligned}$$

Using perturbations of the form  $\delta f(t, \mathbf{r}) = \delta f(z) \exp[ikx + \gamma t]$ , where  $k$  and  $\gamma$  denote the wavenumber along the x-direction and the growth rate of a given mode, respectively, and considering an equilibrium defined by the magnetic field profiles  $B_0(z)$  and  $B_g(z)$ , zero equilibrium velocity, and uniform  $\beta_0$  and  $\Delta\beta_0$ , after a relatively cumbersome derivation, we arrive at the final set of linearized CGL-MHD equations. To improve clarity, we have marked the contributions from different processes, such as the pressure difference perturbation, the equilibrium pressure anisotropy, and the non-ideal terms:

$$\begin{aligned} \gamma \delta v_y = & \underbrace{ikB_0 \delta B_y + B'_g \delta B_z}_{\text{ideal MHD part}} \underbrace{- ikB_0 B_g \delta \Delta p}_{\text{pressure anisotropy fluctuations}} \\ & - \underbrace{\frac{\Delta\beta_0}{2} [ikB_0 (1 - 2B_g^2) \delta B_y + B'_g \delta B_z + 2B_0^2 B_g \delta B'_z]}_{\text{equilibrium pressure anisotropy}} \\ & + \underbrace{\nu (\delta v_y'' - k^2 \delta v_y)}_{\text{viscous part}} \end{aligned} \quad (5)$$

$$\begin{aligned} \gamma (\delta v_z'' - k^2 \delta v_z) = & \underbrace{ik [B_0 (\delta B_z'' - k^2 \delta B_z) - B_0'' \delta B_z]}_{\text{ideal MHD part}} \quad (6) \\ & - \underbrace{k^2 B_0 [2B_0' \delta \Delta p + B_0 \delta \Delta p']}_{\text{pressure anisotropy fluctuations}} \\ & - \underbrace{\frac{\Delta\beta_0}{2} \{ ik [B_0 (\delta B_z'' - k^2 \delta B_z) - B_0'' \delta B_z] }_{\text{equilibrium pressure anisotropy}} \\ & - 2 [ikB_0^2 [B_0 \delta B_z'' + 3B_0' \delta B_z']}_{\text{equilibrium pressure anisotropy}} \\ & + k^2 B_0^2 B_g \delta B_y' + k^2 B_0 [B_0 B_g' + 2B_0' B_g] \delta B_y \}_{}}_{\text{equilibrium pressure anisotropy}} \\ & + \underbrace{\nu (\delta v_z'''' - 2k^2 \delta v_z'' + k^4 \delta v_z)}_{\text{viscous part}} \end{aligned}$$

$$\gamma \delta B_y = \underbrace{ikB_0 \delta v_y - B'_g \delta v_z}_{\text{ideal MHD part}} + \underbrace{\eta (\delta B_y'' - k^2 \delta B_y)}_{\text{resistive part}} \quad (7)$$

$$\gamma \delta B_z = \underbrace{ikB_0 \delta v_z}_{\text{ideal MHD part}} + \underbrace{\eta (\delta B_z'' - k^2 \delta B_z)}_{\text{resistive part}} \quad (8)$$

$$\begin{aligned} \gamma k \delta \Delta p = & \underbrace{\frac{3}{2} \beta_0 k B_0 (B_0 \delta v_z' - ik B_g \delta v_y)}_{\text{plasma-}\beta \text{ dependence}} \quad (9) \\ & + \underbrace{\Delta\beta_0 k B_0 (B_0 \delta v_z' - ik B_g \delta v_y)}_{\text{equilibrium pressure anisotropy}} \\ & - 2\eta \{ \underbrace{3 (B_g B_0' - B_0 B_g')}_{\text{Ohmic heating}} \{ k (B_0' \delta B_y - B_0 \delta B_y') \} \\ & + i \underbrace{[B_g (\delta B_z'' - k^2 \delta B_z) - B_g' \delta B_z']}_{\text{Ohmic heating}} \} \\ & - \underbrace{(B_g B_0' - B_0 B_g') (i B_0 \delta B_z' + k B_g \delta B_y)}_{\text{Ohmic heating}} \\ & + \underbrace{[k B_g' \delta B_y' + i B_0' (\delta B_z'' - k^2 \delta B_z)]}_{\text{Ohmic heating}} \} \end{aligned}$$

In the above equations, ', ', and '''' denote the first-, second-, and fourth-order derivatives with respect to  $z$ , respectively.

\* gabriel.ferreira@inpe.br

† grzegorz.kowal@usp.br

‡ dfalceta@usp.br

- [1] H. P. Furth, J. Killeen, and M. N. Rosenbluth, Finite-Resistivity Instabilities of a Sheet Pinch, *Physics of Fluids* **6**, 459 (1963).
- [2] S. D. Baalrud, A. Bhattacharjee, and Y. M. Huang, Reduced magnetohydrodynamic theory of oblique plasmoid instabilities, *Physics of Plasmas* **19**, 022101 (2012), arXiv:1201.0313 [physics.plasm-ph].
- [3] C. Shi, M. Velli, F. Pucci, A. Tenerani, and M. E. Innocenti, Oblique Tearing Mode Instability: Guide Field and Hall Effect, *The Astrophysical Journal* **902**, 142 (2020), arXiv:2007.00607 [physics.plasm-ph].
- [4] F. Pucci, M. Velli, and A. Tenerani, Fast Magnetic Reconnection: "Ideal" Tearing and the Hall Effect, *The Astrophysical Journal* **845**, 25 (2017), arXiv:1704.08793 [astro-ph.SR].
- [5] L. Ofman, X. L. Chen, P. J. Morrison, and R. S. Steinolfson, Resistive tearing mode instability with shear flow and viscosity, *Physics of Fluids B* **3**, 1364 (1991).
- [6] A. Tenerani, A. F. Rappazzo, M. Velli, and F. Pucci, The Tearing Mode Instability of Thin Current Sheets: the Transition to Fast Reconnection in the Presence of Viscosity, *The Astrophysical Journal* **801**, 145 (2015), arXiv:1412.0047 [physics.plasm-ph].
- [7] X. L. Chen and P. J. Morrison, The effect of viscosity on the resistive tearing mode with the presence of shear flow, *Physics of Fluids B* **2**, 2575 (1990).
- [8] Q. Chen, A. Otto, and L. C. Lee, Tearing instability, Kelvin-Helmholtz instability, and magnetic reconnection, *Journal of Geophysical Research* **102**, 151 (1997).
- [9] C. P. Escoubet, M. Fehringer, and M. Goldstein, Introduction: The Cluster mission, *Annales Geophysicae* **19**, 1197 (2001).

- [10] V. Angelopoulos, The THEMIS Mission, *Space Science Reviews* **141**, 5 (2008).
- [11] J. L. Burch, T. E. Moore, R. B. Torbert, and B. L. Giles, Magnetospheric Multiscale Overview and Science Objectives, *Space Science Reviews* **199**, 5 (2016).
- [12] B. H. Mauk, N. J. Fox, S. G. Kanekal, R. L. Kessel, D. G. Sibeck, and A. Ukhorskiy, Science Objectives and Rationale for the Radiation Belt Storm Probes Mission, *Space Science Reviews* **179**, 3 (2013).
- [13] S. D. Bale *et al.*, Highly structured slow solar wind emerging from an equatorial coronal hole, *Nature* **576**, 237 (2019).
- [14] J. C. Kasper *et al.*, Alfvénic velocity spikes and intense currents within magnetically-linked flux rope structures during parker solar probe’s encounter, *The Astrophysical Journal Letters* **873**, L12 (2019).
- [15] O. Khabarova, T. Sagitov, R. Kislov, and G. Li, Automated Identification of Current Sheets—A New Tool to Study Turbulence and Intermittency in the Solar Wind, *Journal of Geophysical Research (Space Physics)* **126**, e29099 (2021), arXiv:2101.02804 [physics.space-ph].
- [16] Y. S. Ge, J. P. McFadden, J. Raeder, V. Angelopoulos, D. Larson, and O. D. Constantinescu, Case studies of mirror-mode structures observed by THEMIS in the near-Earth tail during substorms, *Journal of Geophysical Research (Space Physics)* **116**, A01209 (2011).
- [17] S. P. Gary, B. Lavraud, M. F. Thomsen, B. Lefebvre, and S. J. Schwartz, Electron anisotropy constraint in the magnetosheath: Cluster observations, *Geophysical Research Letters* **32**, L13109 (2005).
- [18] L. C. Tan, S. F. Fung, R. L. Kessel, S. H. Chen, J. L. Green, and T. E. Eastman, Ion temperature anisotropies in the Earth’s high-latitude magnetosheath: Hawkeye observations, *Geophysical Research Letters* **25**, 587 (1998).
- [19] L. N. Hau and U. O. Sonnerup, On slow-mode waves in an anisotropic plasma, *Geophysical Research Letters* **20**, 1763 (1993).
- [20] B. U. O. Sonnerup, The Reconnecting Magnetosphere, in *Magnetospheric Physics*, Astrophysics and Space Science Library, Vol. 44 (1974) p. 23.
- [21] S. Chiou and L. Hau, The Resistive Tearing-Mode Instability in Anisotropic Plasmas: Linear Theory, in *AGU Spring Meeting Abstracts*, Vol. 2001 (2001) pp. SM42B–08.
- [22] S. W. Chiou and L. N. Hau, Tearing-mode instability in anisotropic plasmas: Effects of energy closure, *Geophysical Research Letters* **29**, 1815 (2002).
- [23] S. W. Chiou and L. N. Hau, Explosive and oscillatory tearing-mode instability in gyrotropic plasmas, *Physics of Plasmas* **10**, 3813 (2003).
- [24] G. F. Chew, M. L. Goldberger, and F. E. Low, The Boltzmann Equation and the One-Fluid Hydromagnetic Equations in the Absence of Particle Collisions, *Proceedings of the Royal Society of London Series A* **236**, 112 (1956).
- [25] L. N. Hau, A note on the energy laws in gyrotropic plasmas, *Physics of Plasmas* **9**, 2455 (2002).
- [26] T. Berlok and C. Pfrommer, On the Kelvin-Helmholtz instability with smooth initial conditions - linear theory and simulations, *Monthly Notices of the Royal Astronomical Society* **485**, 908 (2019), arXiv:1902.01403 [astro-ph.GA].
- [27] D. Falceta-Gonçalves and G. Kowal, Fast Magnetic Field Amplification in the Early Universe: Growth of Collisionless Plasma Instabilities in Turbulent Media, *The Astrophysical Journal* **808**, 65 (2015), arXiv:1506.06398 [astro-ph.CO].